Two-stage XOR electro-optic directed logic gates based on a reflective-type microring resonator

Zhizhi Yang[a], Simin Li*[a], Menghao Huang[a], Zhenzhou Tang[a], Shilong Pan[a]
[a]Key Laboratory of Radar Imaging and Microwave Photonics, Ministry of Education, Nanjing University of Aeronautics and Astronautics, Nanjing 210016, China

ABSTRACT

A cavity-based two-stage XOR electro-optic directed logic scheme using a novel reflective-type microring resonator is proposed and simulated. The proposed design with only one microring resonator used has a smaller footprint, better robustness, and less workload for initialization than previous works.

Keywords: Microring resonator, Optical logic gates, Optical computing, Integrated optics, optical signal processing

1. INTRODUCTION

The serial nature of the conventional Boolean logic circuits is one of the significant obstacles of paving the way for ultra-fast computation[1,2]. Although the propagation delay induced by the electrical logic gates can be further reduced, it will eventually encounter its bottleneck. To mitigate the impediment above, the concept of electro-optic directed logic taking advantage of the fast-speed and ultra-low-loss properties of light has emerged as one of the promising digital logic paradigms[3,4].

Extensive researches have been conducted in the past on implementing electro-optic logic gates through resonant cavities. These devices usually consist of cascaded microring resonators (MRRs) or other optical cavity and conduct logic computation with electrical inputs and optical outputs. Compared to the nonlinear method of optical logic, cavity-based approach is easy to achieve and energy-efficient[4]. However, several issues remain. The first issue is the complexity of the parameter control for microrings obtaining the proper state; secondly, several MRRs may occupy a large footprint[5–7]. Previously, we proposed a novel reflective-type microring resonator (RT-MRR), enabling reconfigurable photonic integrated circuits such as photonic microwave filter and optical delayline[8,9]. Afterward, we reported a single-stage XNOR/XOR electro-optic logic gate based on an RT-MRR[10].

Here, distinguished from our previous work, we propose an electro-optic directed logic scheme of two-stage XOR gates on an RT-MRR by controlling the phase shift of the MZI couplers. Although it is a two-stage logic gate, the proposed device does not bring inter-stage latency since we realize the logic computation optically.

2. OPERATION PRINCIPLE AND RESULT

Figure 1 shows the schematic of the RT-MRR. It consists of a conventional add-drop microring and a reflector connected to the Port 3 (Drop). The light enters the proposed device through Port 1 (Input) and outputs from Port 4 (Output). The frequency of the injecting light signal is pre-set coinciding with one of the RT-MRR's resonant frequency. Two Mach-Zehnder interferometer (MZI) couplers with thermo-optic heaters or other modulation schemes are employed to control the output state of the RT-MRR. Recently, we have demonstrated a single-stage XOR electro-optic logic gate[10]; the logic expression generates at the Port 4 (Output) as optical intensity. The control signals are the coupling coefficients. Since the coupling coefficients are decided from the phase shift applied to MZI coupler, the previously proposed device can be recognized as a phase-shift-controlled electro-optic logic. Here, we use the MZI coupler as a tunable coupler to adjust the coupling coefficient of the microring resonator as well as using its symmetry of the transfer function to implement a logic operation. The first stage of the proposed two-stage electro-optic XOR logic gates is implemented by the upper MZI coupler, annotated as MZI 1 in Figure 1.

*lisimin@nuaa.edu.cn

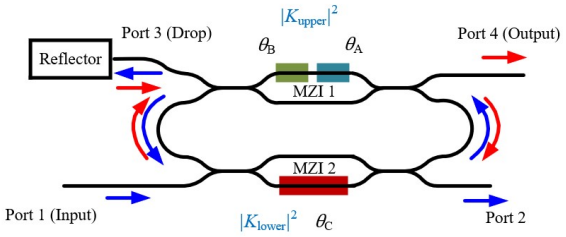

Figure 1. Schematic of the reflective-type microring resonator.

As a versatile basic structure in the realm of photonics integrated circuit, various applications can be achieved using Mach-Zehnder Interferometer (MZI) coupler including optical filter, switch, optical modulator, sensor, and tunable coupler.

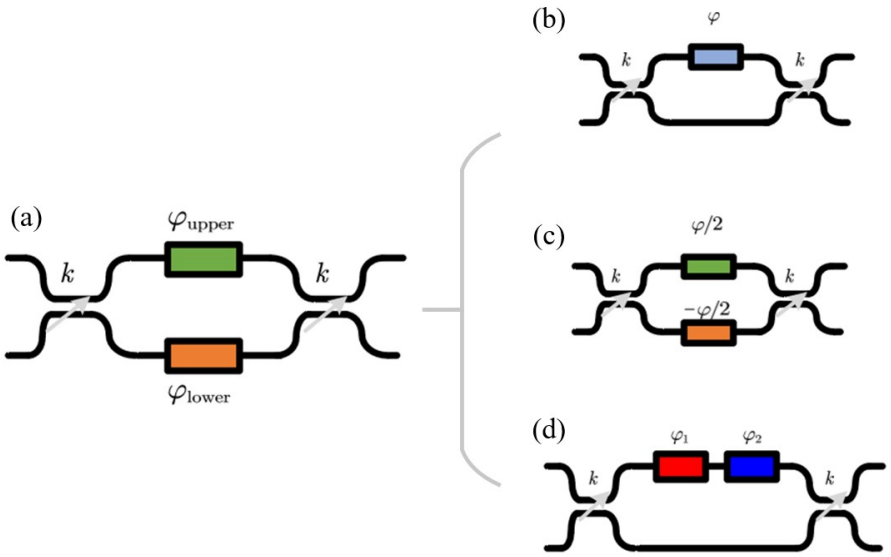

Figure 2. Mach-Zehnder Interferometer coupler with different phase-shifting schemes, (a) Single-arm phase-shift MZI coupler, (b) Push-pull phase-shift MZI coupler, (c) An alternative of single-arm phase-shift MZI coupler with two phase shifters on the same arm

Figure 2 show the general MZI coupler and its typical variants using different phase-shifting schemes. Generally, an MZI coupler consists of two directional couplers connected by two waveguides with phase shifter as shown in Figure 2(a). Assuming that the transmission phase and the coupling ratio of the directional coupler k are independent of the tunable phase shifter, the coupling coefficient $|K(\varphi_{\text{upper}}, \varphi_{\text{lower}})|^2$ of the general MZI coupler is given by

$$|K(\varphi_{\text{upper}}, \varphi_{\text{lower}})|^2 = |j\sqrt{k(1-k)} \cdot (e^{j\varphi_{\text{upper}}} + e^{j\varphi_{\text{lower}}})|^2 \tag{1}$$

Shown in Figure 2(b), the single-arm phase-shift MZI coupler is a special case when $\varphi_{\text{lower}} = 0$. It has only one phase shifter placed asymmetrically on one arm of the MZI coupler. Based on the Equation (1), the coupling coefficient $|K|^2$ for single-arm phase-shift MZI coupler is given by

$$\begin{aligned} |K(\varphi)|^2 &= |j\sqrt{k(1-k)} \cdot (e^{j\varphi} + 1)|^2 \\ &= a \cdot (1 + \cos\varphi) \end{aligned} \tag{2}$$

where $a = 2k(1-k)$. Without the loss of the generality, we assume the $k = 0.5$ and

$$|K(\varphi)|^2_{k=0.5} = \frac{1}{2} + \frac{1}{2}\cos\varphi \tag{3}$$

For the push-pull phase-shift MZI coupler, as shown in Figure 2 (c), the phase shifts applied to the arms are inverted. We defined the phase shift on one arm as $\varphi/2$, and therefore the phase difference between two arms of the MZI coupler as

$$\varphi = \varphi/2 - (-\varphi/2) \tag{4}$$

The transfer function when $k = 0.5$ is given by

$$\begin{aligned} |K(\frac{\varphi}{2})|^2_{k=0.5} &= |j\sqrt{a/2} \cdot (e^{j\varphi/2} + e^{j\varphi/2})|^2 \\ &= \frac{1}{2} + \frac{1}{2}\cos\varphi \end{aligned} \tag{5}$$

The same functionality of tuning coupling coefficient can be realized with the push-pull phase-shift MZI coupler with smaller drive voltages compared to the single-arm phase-shift MZI coupler.

Figure 2 (d) shows an alternative of single-arm phase-shift MZI couple. Compared to the original single-arm phase-shift MZI coupler, the alternative one utilizes two phase shifters on one arm of the MZI coupler. The phase shifts brought by the phase shifter shown in Figure 2 (d) are φ_1 and φ_2. The transfer function of the alternative when $k = 0.5$ is given by

$$|K(\varphi_1, \varphi_2)|^2_{k=0.5} = \frac{1}{2} + \frac{1}{2}\cos(\varphi_1 + \varphi_2) \tag{6}$$

In this proposed device, a single-arm phase-shift and an alternative of single-arm phase-shift MZI coupler are implemented to control the status of the MRR.

Figure 3 shows the transfer function of the single-arm phase-shift MZI coupler varying with the phase shift. Since the transfer function is symmetric to a specific phase, which is 2π here, two separated phase shifts can be obtained for the same coupling coefficient.

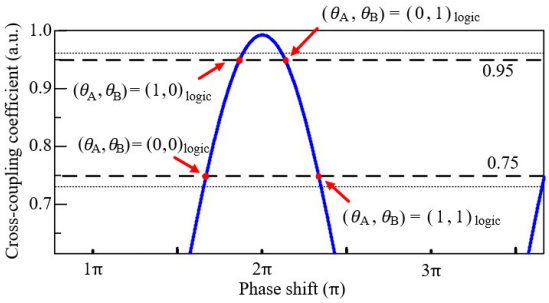

Figure 3. The transfer function of an MZI coupler in the reflective-type microring resonator.

Using the alternative of single-arm phase-shift MZI coupler with two phase shifters on the same arm and applying the phase shifts separately, we can obtain a logic relationship from the sets of (θ_A, θ_B) to coupling coefficient of the MZI coupler. The coupling coefficient of the MZI 1 is also the upper cross-coupling coefficients of the RT-MRR. When the $\theta_A = 0$ and $\theta_B = 1.6667 \cdot \pi$, which is corresponding to the logic input $(0, 0)_{logic}$, the cross-coupling coefficient is 0.75. Also, when the $\theta_A = 0.1897 \cdot \pi$ and $\theta_B = 2.1435 \cdot \pi$, corresponding to the logic input $(1, 1)_{logic}$, the cross-coupling coefficient is mapped to 0.75. Similarly, when the inputs of (θ_A, θ_B) is $(0, 1)_{logic}$ or $(1, 0)_{logic}$, both cross-coupling coefficients are mapped to 0.95. The phase-shift values for the MZI coupler are shown in Table 1 and the truth table is shown in Table 2. The relationship between the logic input of (θ_A, θ_B) and the upper cross-coupling coefficient, therefore, is equivalent to an XOR logic. Therefore, the alternative of single-arm phase-shift MZI coupler form the first stage of the logics in the proposed device.

Table 1 The phase values of (θ_A, θ_B)

	Phase at $(0)_{logic}$	Phase at $(1)_{logic}$
θ_A	0	$0.1897\cdot\pi$
θ_B	$1.6667\cdot\pi$	$2.1435\cdot\pi$

Table 2 The truth table of the first stage of electro-optic logic gates

θ_A	θ_B	Cross-coupling Coefficient (Upper)
0	0	$0.75, (0)_{logic}$
0	1	$0.95, (1)_{logic}$
1	1	$0.75, (0)_{logic}$
1	0	$0.95, (1)_{logic}$

The second stage of the logics is obtained based on the scheme like our previous work[6]. The inputs and the outputs are the coupling coefficients and the optical intensity of the RT-MRR's output port at the resonant wavelength respectively. We define the phase shift of the MZI 2 as θ_C. By applying different phase values of θ_C, according to Equation (3), we can control the lower coupling coefficient of the RT-MRR. Since the relation between the coupling coefficients and optical intensity at the resonant wavelength of the RT-MRR can be an XOR logic, we can realize the second-stage XOR electro-optic directed logic.

Finally, employing the phases θ_A, θ_B, and θ_C as three control variables, we can obtain a two-stage XOR electro-optic directed logics, as shown in Figure 4.

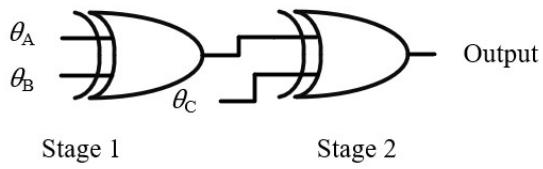

Figure 4. Schematic of two-stage XOR logic gates.

To verify the feasibility of our model, a numerical simulation based on the transmission matrix formalism is conducted[11,12]. The effective index of the waveguide is set to be 3.24, and the radius is set to 100 μm. Then, we apply sets of phase shift's values and obtain the intensity responses of each set values, as shown in Figure 5 and Table 3 below. The result shows the logic relationship between the phases θ_A, θ_B, and θ_C and the optical intensity at the resonant wavelength of the RT-MRR. Through the analysis of the data, we can conclude the truth table as shown in Table 4 and Table 5. The result proves that the relationship between the phases θ_A, θ_B, and θ_C and the optical intensity at the resonant wavelength of the RT-MRR form a two-stage XOR electro-optic directed logics, as shown in Figure 4.

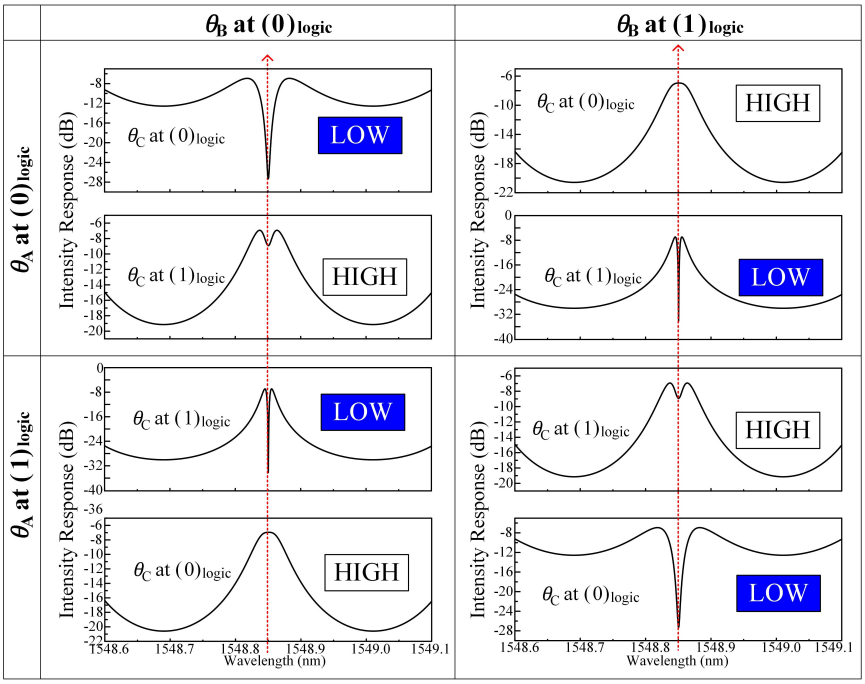

Figure 5. The intensity responses of the RT-MRR under each set of phase shift input.

Table 3 The phase values of θ_A, θ_B, and θ_C at the states of $(0)_{logic}$ and $(1)_{logic}$.

θ_i	θ_i at $(0)_{logic}$	θ_i at $(1)_{logic}$
θ_A	0	$0.1897 \cdot \pi$
θ_B	$1.6667 \cdot \pi$	$2.1435 \cdot \pi$
θ_C	$1.6579 \cdot \pi$	$1.8651 \cdot \pi$

Table 4 The truth table of the proposed two-stage XOR when $\theta_C = (0)_{logic}$

Input, $\theta_C = (0)_{logic}$		Output (Optical intensity at the resonant wavelength)
θ_A	θ_B	
0	0	0
0	1	1
1	0	1
1	1	0

Table 5 The truth table of the proposed two-stage XOR when $\theta_C = (1)_{logic}$

Input, $\theta_C = (1)_{logic}$		Output (Optical intensity at the resonant wavelength)
θ_A	θ_B	
0	0	1
0	1	0
1	0	0
1	1	1

3. CONCLUSION

In summary, we have proposed a cavity-based two-stage electro-optic XOR logic gates using an RT-MRR. The point of our scheme is using an MZI coupler as the first stage of the logic gates and the RT-MRR as the second stage of the logic gates. To achieve the first stage, an alternative of single-arm phase-shift Mach-Zehnder Interferometer coupler is used to obtain the XOR logic relationship from the phase-shift values to the coupling coefficient based on the symmetry of the MZI's transfer function. Then, the second stage of the logics is realized by controlling the coupling coefficients of the RT-MRR. The proposed method is demonstrated through simulation, in which the intensity response under different sets of the phase shift is perfectly mapped to the intensity response at the resonant wavelength, proved the feasibility of our proposed scheme.

Compared to previous cavity-based electro-optic logic gates, one of the advantages of our device is saving footprint. The conventional cascaded microring scheme will require twice the amount of microrings for the same result. Furthermore, the halved amount of microrings not only reduces the manufacturing difficulty and the tuning workload, but also pave the way for further large-scale applications.

ACKNOWLEDGEMENT

This work was supported by the National Key R&D Program of China (2018YFB2201803), the National Natural Science Foundation of China (No. 61604072), China Postdoctoral Science Foundation (No. 2016M590450).

REFERENCES

[1] Caulfield, H. J. and Dolev, S., "Why future supercomputing requires optics," Nat. Photonics 4(5), 261–263 (2010).
[2] Minzioni, P., Lacava, C., Tanabe, T., Dong, J., Hu, X., Csaba, G., Porod, W., Singh, G., Willner, A. E., Almaiman, A., Torres-Company, V., Schroder, J., Peacock, A. C., Strain, M. J., Parmigiani, F., Contestabile, G., Marpaung, D., Liu, Z., Bowers, J. E., et al., "Roadmap on all-optical processing," J. Opt. 21(6), 063001 (2019).
[3] Hardy, J. and Shamir, J., "Optics inspired logic architecture," Opt. Express 15(1), 150 (2007).
[4] Cutrona, L. J., Leith, E. N., Palermo, C. J. and Porcello, L. J., "Optical Data Processing and Filtering Systems," IRE Trans. Inf. Theory 6(3), 386–400 (1960).
[5] Zhang, L., Ji, R., Jia, L., Yang, L., Zhou, P., Tian, Y., Chen, P., Lu, Y., Jiang, Z., Liu, Y., Fang, Q. and Yu, M., "Demonstration of directed XOR/XNOR logic gates using two cascaded microring resonators," Opt. Lett. 35(10), 1620 (2010).
[6] Fushimi, A. and Tanabe, T., "All-optical logic gate operating with single wavelength," Opt. Express 22(4), 4466 (2014).
[7] Qi, Y., Qiu, C., Gao, W., Zhong, X. and Su, Y., "Silicon Reconfigurable Electro-Optical Logic Circuit Enabled by a Single-Wavelength Light input," IEEE Photonics Technol. Lett. 31(6), 1–1 (2019).
[8] Huang, M., Li, S., Xue, M., Zhao, L. and Pan, S., "Flat-top optical resonance in a single-ring resonator based on manipulation of fast- and slow-light effects," Opt. Express 26(18), 23215 (2018).

[9] Huang, M., Li, S., Yang, Z. and Pan, S., “Analysis of a flat-top optical ring resonator,” Opt. Commun. 451(June), 290–295 (2019).
[10] Pan, S., Tang, Z., Huang, M. and Li, S., “Reflective-type microring resonator for on-chip reconfigurable microwave photonic systems,” IEEE J. Sel. Top. Quantum Electron. 26(5), 1–12 (2020).
[11] Heebner, J. E., Grover, R. and Ibrahim, T. A., [Optical microresonators: theory, fabrication, and applications], Springer, London (2008).
[12] Bogaerts, W., De Heyn, P., Van Vaerenbergh, T., De Vos, K., Kumar Selvaraja, S., Claes, T., Dumon, P., Bienstman, P., Van Thourhout, D. and Baets, R., “Silicon microring resonators,” Laser Photonics Rev. 6(1), 47–73 (2012).